Supplementary Materials for

Structural basis for coupling of protein transport and N-glycosylation at the mammalian endoplasmic reticulum

Katharina Braunger, Stefan Pfeffer, Shiteshu Shrimal, Reid Gilmore, Otto Berninghausen, Elisabet Mandon, Thomas Becker, Friedrich Förster, Roland Beckmann

correspondence to: beckmann@genzentrum.lmu.de, pfeffer@biochem.mpg.de, f.g.forster@uu.nl

This PDF file includes:

Other Supplementary Materials for this manuscript includes the following:

Materials and Methods

Preparation of rough microsomes from HEK cells for cryo-ET

Rough microsomes were prepared from 20 confluent 100-mm plates of STT3 A -/-, STT3 B -/- or wild type HEK293 cells as previously described (*10*). Briefly, the cells were detached by trypsinization, washed twice with PBS and centrifuged at 600 x *g* for 5 min. Then, the cells were incubated in buffer A (10 mM Hepes, pH 7.6, 1 mM EGTA, 25 mM KOAc, 2.5 mM $Mg(OAc)_2$, 0.1U/ml RNAsin,1 ug/ml cycloheximide (CHX) and 1x PIC (protease inhibitor cocktail)) for 20 min at 4°C and centrifuged at 600 x *g* for 5 min. The cell pellets were resuspended in buffer A and adjusted to 250 mM sucrose using 20 strokes of a dounce homogenizer. The cell homogenates were centrifuged at 1,000 x *g* for 10 min, and the supernatants were recentrifuged at 12,000 x *g* for 15 min to remove the mitochondrial fraction. The rough microsomes were purified from the post mitochondrial supernatants by a sucrose step cushion (600 mM sucrose in Buffer A, 90 min, 192697 x *g* avg in a Type 70.1 Ti). Finally, the rough microsomal membranes were resuspended in 50 mM Hepes pH 7.6, 100 mM KOAc, 250 mM sucrose, 5 mM Mg $(OAc)_2$ and, 0.1U/ml RNAsin,1 ug/ml CHX and 1x PIC. Rough microsomal membranes from wild type or mutant HEK293 cells (20 µg) were resolved by SDS-PAGE and analyzed by immunoblotting using rabbit polyclonal antibodies against the C terminus of human STT3A (residues 693-705) (*9*) or the recombinantly expressed 73 N-terminal residues of human STT3B (*11*).

Purification of ribosome-nascent-chain translocon complexes for cryo-EM SPA

Canine puromycin/high-salt treated rough membranes (PKRM) were prepared as described before (*23*). In vitro translation was performed using a nuclease treated reticulocyte lysate system (Promega) supplemented with 400 U/mL RNasin (Ambion). 30 µg mRNA encoding for amino acids 1-75 of bovine opsin with an N-terminal HA tag and a C-terminal hCMV stalling sequence were added to 300 µL of translation reaction and incubated at 28°C for 30 min. 17 eq PKRM were pretreated with 240 U of RNasin for 5 min prior to addition to the translation mix and added to the translation mix 5 minutes after addition of mRNA. Translation was stopped by addition of 0.2 µg/µL CHX. Subsequently the concentration of potassium acetate in the reaction mix was increased to 500 mM and incubated for 30 min at 25°C. Membranes were isolated by pelleting through a sucrose cushion (0.5 M sucrose, 30 mM HEPES/KOH pH 7.5, 10 mM $Mg(OAc)_2$, 500 mM KOAc/HAc pH 7.4, 1 mM DTT, 10 µg/mL CHX) in a TLA120.2 rotor for 10 min at 47,446 x *g* at 4°C and dissolved in solubilization buffer S (30 mM HEPES/KOH 7.5, 10 mM $Mg(OAc)_2$, 100 mM KOAc/HAc 7.4 , 1.5% digitonin, 1 mM DTT, 10 µg/mL CHX) for 45 min at 25°C. Solubilized ribosome-translocon complexes were pelleted through a sucrose cushion (0.5 M sucrose, 30 mM HEPES/KOH pH 7.5, 10 mM $Mg(OAc)_2$, 100 mM KOAc/HAc pH 7.4, 0.3% digitonin, 1 mM DTT, 10 µg/mL CHX) in a TLA 120.2 rotor for 45 min at 355,040 g at 4°C. The isolated complexes were resuspended in buffer E (30 mM HEPES/KOH 7.5, 10 mM $Mg(OAc)_2$, 100 mM KOAc/HAc pH 7.4, 0.3% digitonin, 1 mM DTT, 10 µg/mL CHX) and used for cryo-EM analysis.

Grid preparation and data acquisition for cryo-ET

Rough microsomes from HEK cells were diluted in microsome buffer (20 mM Hepes, pH 7.6; 50 mM KCl; 2 mM $MgCl_2$) before 3 µl were applied to lacey carbon molybdenum grids (Ted Pella, USA). An equal volume of 10-nm colloidal gold in microsome buffer was added to the grid and the sample was vitrified in liquid ethane using a Vitrobot Mark IV (FEI Company, The Netherlands) after an incubation time of 20 s at 22°C. Tilt series were acquired using either a FEI Titan Krios (STT3A(-/-) and STT3B(-/-) HEK microsomes) or a FEI Tecnai Polara (wildtype HEK microsomes) transmission electron microscope (TEM). Tilt images were recorded on a K2 Summit direct electron detector (Gatan, USA) in movie mode with 4-7 frames per tilt image. The TEMs were operated at an acceleration voltage of 300 kV, a nominal defocus of 4-5 µm and an object pixel size of 2.62 Å (Titan Krios) or 2.35 Å (Tecnai Polara). Tilt series were acquired from -60° to +60° (first half: -20° to +60°; second half; -22° to -60°) with an angular increment of 2° using the Serial EM acquisition software (*27*). The cumulative electron dose did not exceed 100 electrons/$Å^2$.

Grid preparation and data acquisition for cryo-EM SPA

Carbon coated holey grids (2 nm, Quantifoil) were glow discharged at 0.2 mbar for 30 s. For each grid, 3.5 µL of sample were applied to the grids at a concentration of 5.5 A_{260} ml^{-1}. Subsequent vitrification was performed by plunge freezing in liquid ethane using a Vitrobot mark IV (FEI Company, Netherlands) with a blotting time of 3 s at 4°C.

Cryo-EM data was collected semi-automatically using the acquisition software EM-TOOLS (TVIPS, Germany) on a Titan Krios transmission electron microscope (FEI Company) at a defocus range between 0.9 and 3.5 µm. All data were recorded on a Falcon II detector upgraded with a Falcon III detector chip under low dose conditions with a nominal pixel size of 1.084 Å/pixel on the object scale. A total of 13087 micrographs were collected. All micrographs experienced a total exposure of ~28 electrons/$Å^2$ fractionated into 10 frames.

Image processing for cryo-ET

Rough microsomes from HEK cells: K2 movies were aligned using Motioncor2 (*28*). Tilt series were aligned using gold fiducial markers and weighted back projection was used for tomogram reconstruction (binned object pixel: 2.1 nm) in PyTom (*29*). Template matching was performed against a single particle cryo-EM reconstruction of the human 80S ribosome (*30*) filtered to 5 nm resolution in PyTom (*29*). Subtomograms were directly extracted from microsome-containing tomogram areas at the coordinates of the 500 highest-scoring peaks obtained from template matching. These subtomograms were classified for each tomogram separately using constrained principal component analysis (CPCA) (*31*) focusing on the large ribosomal subunit and the ER membrane. In this first classification step ER membrane-associated ribosomes were separated from most false-positive matches and non-membrane-bound ribosomes. For the retained coordinates, subtomograms were reconstructed at higher spatial resolution using PyTom (110^3 voxels, binned object pixel: 0.542 nm for STT3A(-/-) and STT3B(-/-) HEK microsomes; 128^3 voxels, binned object pixel: 0.47 nm for wildtype HEK microsomes). These subtomograms were iterative aligned using PyTom (*29*) and classified again focusing on the translocon region. This separated different ribosome-translocon populations (Fig. 1). The number of subtomograms used for averaging in each class is indicated in Fig. 1. Subtomogram

averages obtained from wildtype HEK microsomes were resampled to fit the voxel size and coordinate system of subtomogram averages obtained from STT3A(-/-) and STT3B(-/-) HEK microsomes.

Canine pancreatic microsomes: A previously published dataset was re-processed to improve resolution. The processing was performed as published (*18*), with one major exception: we prepared five to seven sets of slightly differently aligned projections to account for local distortions of the sample geometry, i.e. for each gold fiducial traced in a tomogram, a separate set of aligned projections centered on the respective gold fiducial was prepared. For reconstruction of each subtomogram, we then selected always the set of projections that was aligned centered on the gold fiducial closest to the respective particle coordinates. The final subtomogram average was filtered according to local resolution as determined using Bsoft (*32*). The subtomogram average was resampled to fit the coordinate system of the cryo-EM single particle reconstructions of the solubilized RTCs.

Image processing for cryo-EM SPA

Original image stacks were summed up and aligned at micrograph level using MotionCor2 (*28*). The contrast transfer function parameters were estimated via GCTF (*33*). All micrographs were screened manually for ice quality prior to automated particle picking with Gautomatch (http://www.mrclmb.cam.ac.uk/kzhang). All classifications and refinements were performed using Relion-2.1 (*34*).

Two datasets were collected individually and joined after automated particle picking and reference-free 2D classification. Altogether 1.343.416 ribosomal particles were subjected to extensive 3D classification after an initial round of refinement (Fig. S2). Differences between the resulting eleven classes comprised the presence or absence of the small ribosomal subunit, the OST complex, eEF2 as well as different tRNA states. Also conformational differences in the L1 stalk and the relative arrangement of ribosomal subunits were found. A clean class with densities for both P site tRNA and OST (188.900 particles; 14.1 %) was refined to high resolution (reconstruction A1). Two further classes (13.6 %) were lacking density for tRNAs and instead had strong occupancy of eEF2 as well as partial occupancy of the OST complex. These were subjected to another round of 3D classification using a mask on the ligand region where they clearly separated into populations with or without OST. OST-containing particles (90.895 particles) were refined to high resolution (reconstruction B1).

The local resolution for the membrane bound ligand could be substantially improved for both reconstructions (A and B) by a second round of refinement using a mask on the ligand region (reconstructions A2 and B2). All final reconstructions were subjected to post processing using a wide soft edge mask. This resulted in final resolutions of 3.2 Å (Particle A1), 4.2 Å (Particle A2), 3.3 Å (Particle B1) and 4.7 Å (Particles B2) according to the FSC0.143 criterion following the Relion gold-standard refinement.

Homology modeling and refinement of atomic models

Sec61 was modeled based on the structure of the ‘primed’ state (*21*) (pdb 3j7q) with minor adjustments in the plug region (res. 58-66) and TM10 (res. 436-465). The hinge region (res. 196-242) as well as the N-terminus (res. 1-27) were modeled de novo.

The P-site tRNA and the 60S ribosomal subunit were placed as a rigid body using pdb 3jah (*35*). The region contacting the cytosolic RPN1 domain was manually adjusted in Coot

(*36*). Namely, the C-terminus of eL28 was remodeled and extended by 11 aminoacids and the rRNA H19/H20 was rearranged to fit the electron density.

Homology models for the STT3A transmembrane and luminal domains were created using the PHYRE2 server (*37*) based on the archaeal oligosaccharyltransferase AglB (*13*) (pdb 3waj). The model was manually adjusted in Coot based on electron density features and the recent high resolution yeast oligosaccharyltransferase structure (*15*) (pdb 6ezn).

The four-helix bundle of the RPN1 cytosolic domain and the preceding TM were assigned based on the Jpred4 structure prediction software (*38*). For the well-resolved DC2 segment (local resolution ranging from 3.5-4.2 Å) an atomic model of the 3 TM domains was built based on the jPred4 secondary structure prediction and positioning of bulky side chains.

The three biochemically established subcomplexes (*7*) were initially assigned based on the number of TM segments and the assignment was confirmed by the architecture of the yeast OST complex. (Fig. S7).

Subcomplex I comprises RPN1 (1 TM) and TMEM258 (2 TMs), corresponding to a three-TM bundle, as resolved at the distal side of the OST complex facing away from Sec61 and in close proximity to STT3A TM1. Subcomplex II comprises STT3A (13 TMs), DC2 (3 TMs), OST4 (1 TM) and KCP2 (4 TMs). No extra density for the four TMs of KCP2 was observed, most likely because this subunit dissociated upon solubilization of OST (*10*). Subcomplex III is composed of RPN2 (3 TMs), DAD1 (3 TMs) and OST48 (1 TM) and is covered by the seven-TM bundle on the distal side of STT3A.

Homology models for the OST4 and RPN1 TM-domains were created using the PHYRE2 server based on the yeast OST structure (*15*) and manually adjusted in Coot.

Poly-Ala segments were placed when local resolution did not allow to build an atomic model, namely for the TMs of TMEM258 and Subcomplex III (DAD1, OST48, RPN2), for STT3A-TM9 as well as the loop regions in DC2

The entire translocon model was refined using PHENIX (*39*).

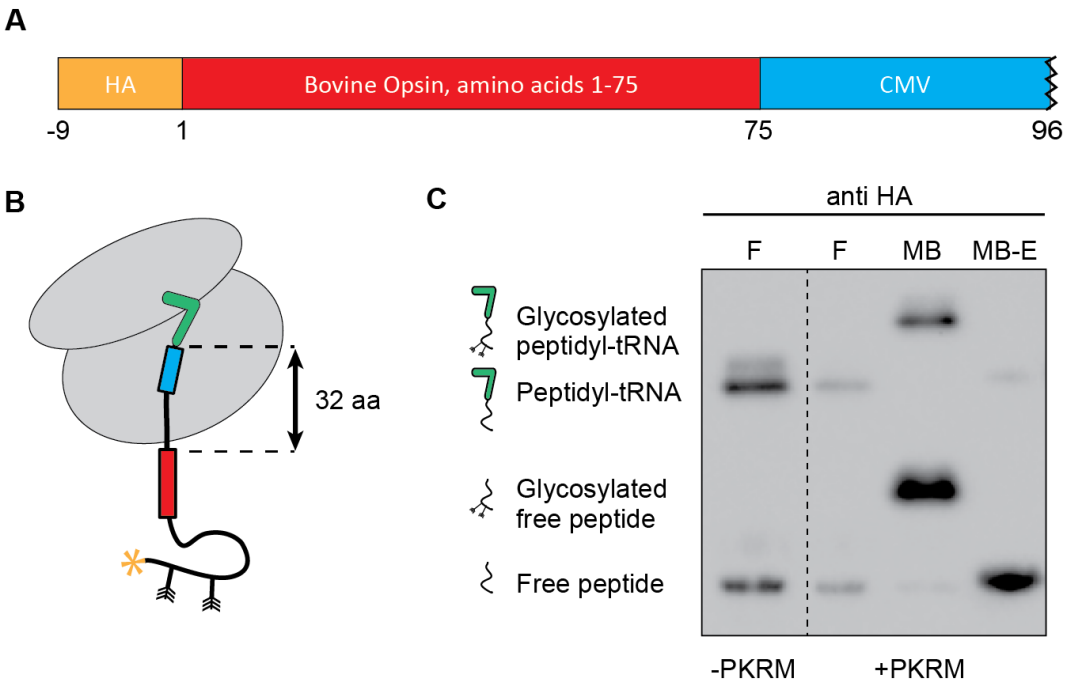

Fig. S1. Characterization of the in vitro N-glycosylation substrate. (A) Schematic representation of the substrate produced by in vitro translation. **(B)** Expected architecture of the stalled ribosome nascent chain complexes generated by in vitro translation-translocation reactions indicating the number of amino acids between the peptidyl-transferase-center and the C-terminus of the first opsin TM segment (red). Double glycosylation is indicated by fletched arrows and the N-terminal HA-Tag is indicated by a yellow asterisk. **(C)** Immuno Blot analysis of in vitro translation assays in absence and presence of dog PKRM after ribosome-pelleting (F=free ribosomes, MB=membrane bound ribosomes, MB-E=membrane bound ribosomes after Endoglycosidase-H treatment).

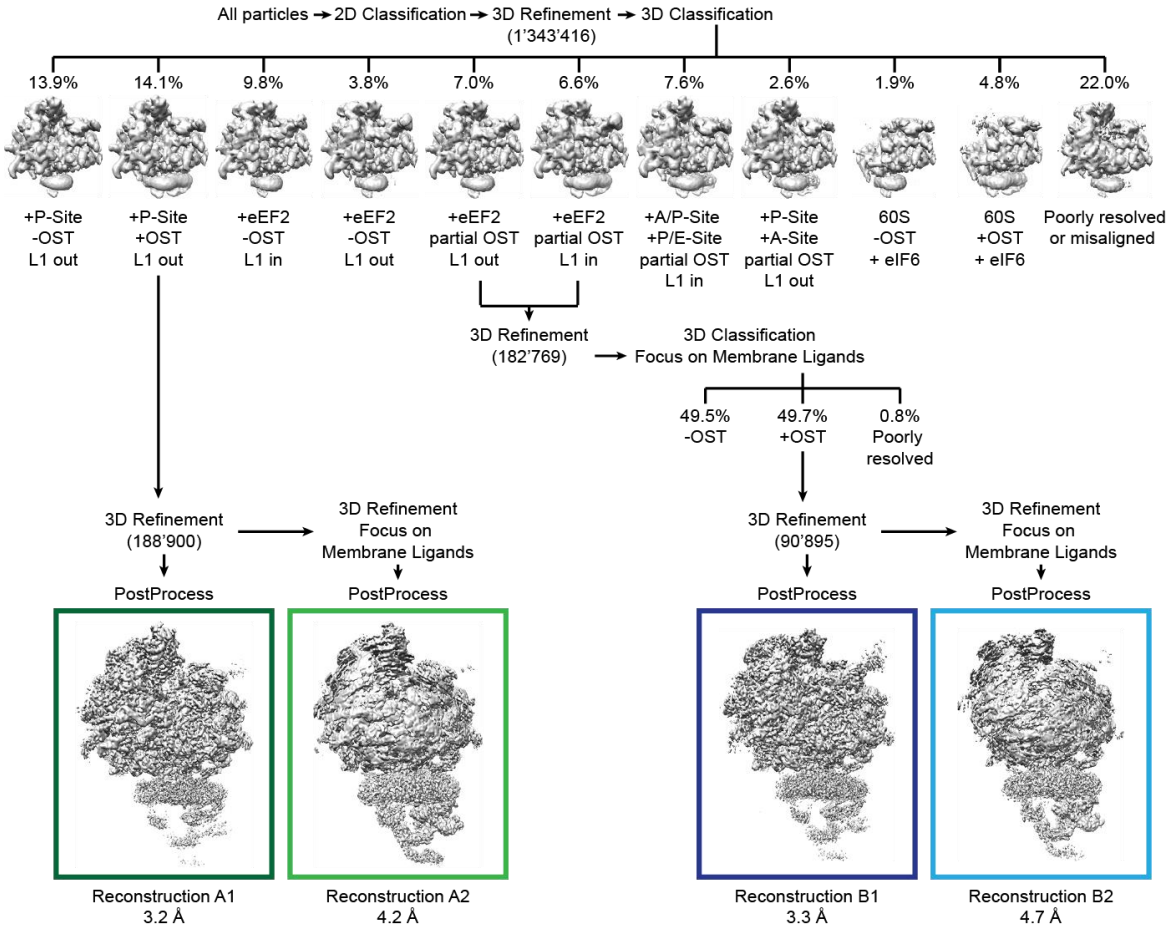

Fig. S2. Classification scheme for SPA of solubilized ribosome-translocon complexes. Two datasets were collected individually and joined after automated particle picking and 2D classification. Initial 3D classification yielded in a clean class with densities for both P site tRNA and OST, which was refined to high resolution (reconstruction A1, dark green). Classes 5 & 6 from the initial 3D classification were lacking density for tRNAs and instead had strong occupancy of eEF2 as well as partial occupancy of the OST complex. They were subjected to another round of 3D classification using a mask on the ligand region where they clearly separated into populations with or without OST. OST-containing particles were refined to high resolution (reconstruction B1, dark blue). The resolution for the membrane bound ligand could be substantially improved for A- and B-Type

reconstructions by a second round of refinement with a mask on the ligand region (Reconstruction A2, light green; B2, light blue).

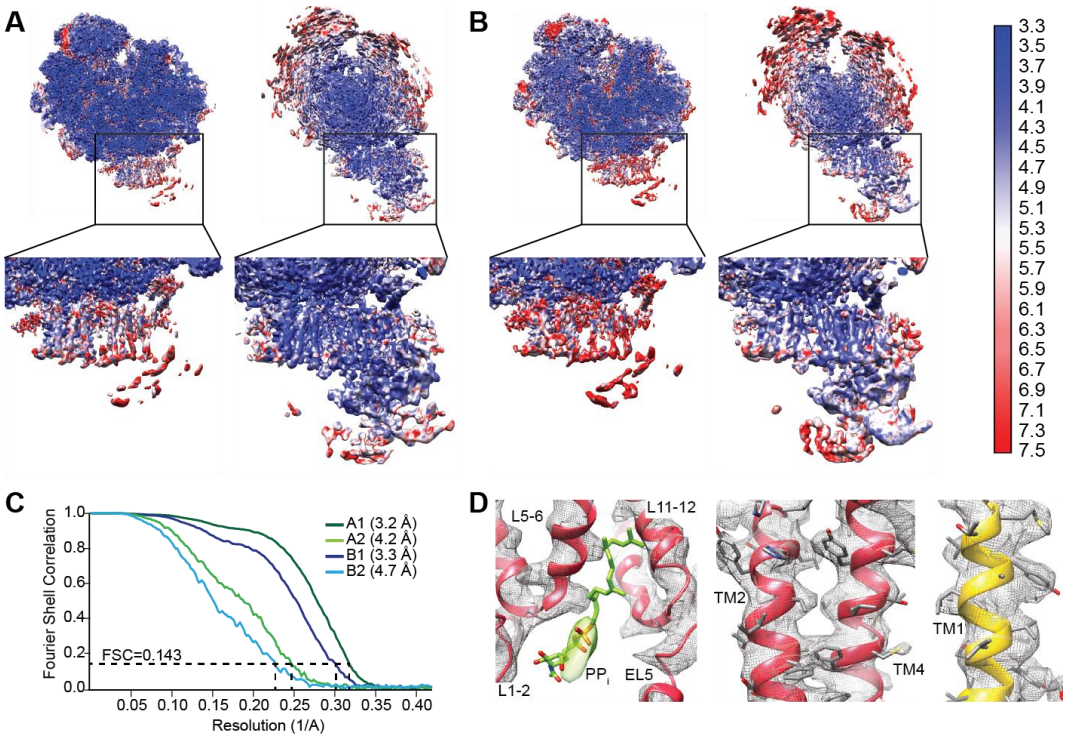

Fig. S3. Quality and resolution of the cryo-EM SPA reconstructions. (A) Maps of P site tRNA containing particles before (left) and after (right) refinement on the ligand region colored according to local resolution. Local refinement significantly improved local resolution in the translocon region to approximately 3.5-4.5 Å for the majority of TM helices. **(B)** Maps of eEF2/OST-containing particles before (left) and after (right) refinement on the ligand region colored by local resolution. **(C)** Fourier shell correlation (FSC) of the cryo-EM SPA maps. Resolution was determined according to the gold-standard criterion (FSC=0.143). **(D)** Example densities with models for STT3 (red), phosphates (green) and DC2 (yellow).

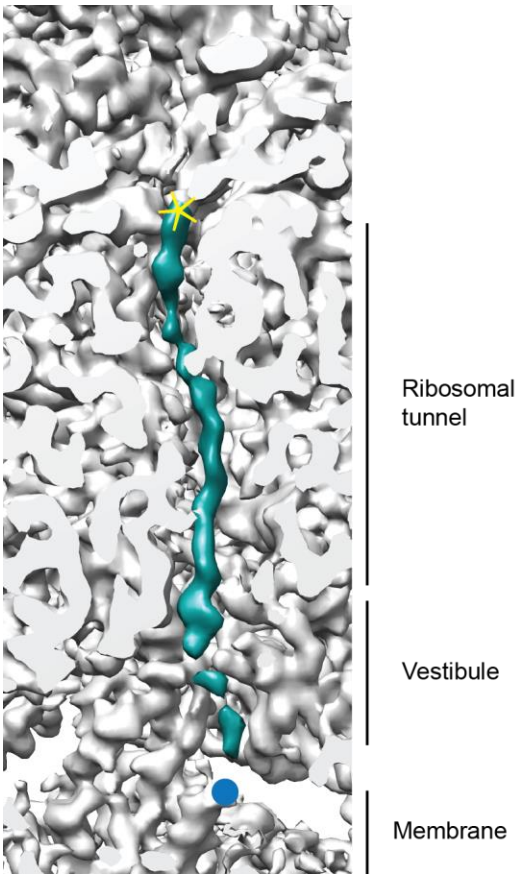

Fig. S4. The peptide exit tunnel in the programmed OST-containing SPA reconstruction. Section through the P-site tRNA containing reconstruction (A1). Map has been filtered to 4.2 Å according to local resolution of the densities in the ribosomal tunnel. Density for the nascent-chain (dark cyan) can be traced from the peptidyl-transferase center (yellow asterisk) through the tunnel vestibule projecting towards the tip of Sec61α TM10 (blue dot).

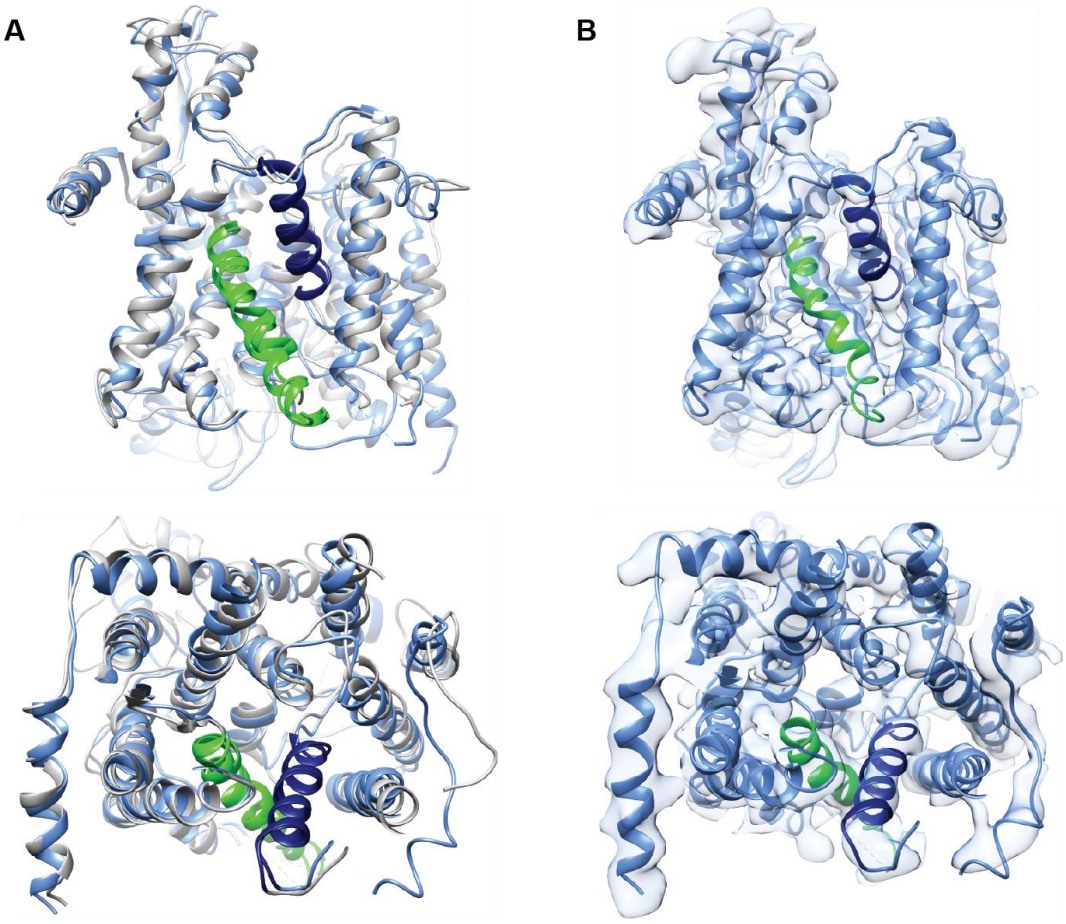

Fig. S5. Sec61 conformation in the ribosome translocon complex. (A) Model of Sec61 (light blue) superimposed to a model of the 'primed' state (light grey, PDB 3j7q). Views perpendicular to the membrane plane (top) and from the cytosol (bottom) are shown. The lateral gate between TM2 (dark blue) and TM7 (green) is in closed conformation. **(B)** Model of Sec61 fitted into the electron density map of reconstruction A1, low-pass filtered according to local resolution at 4.0 Å. Identical views as in **(A)**.

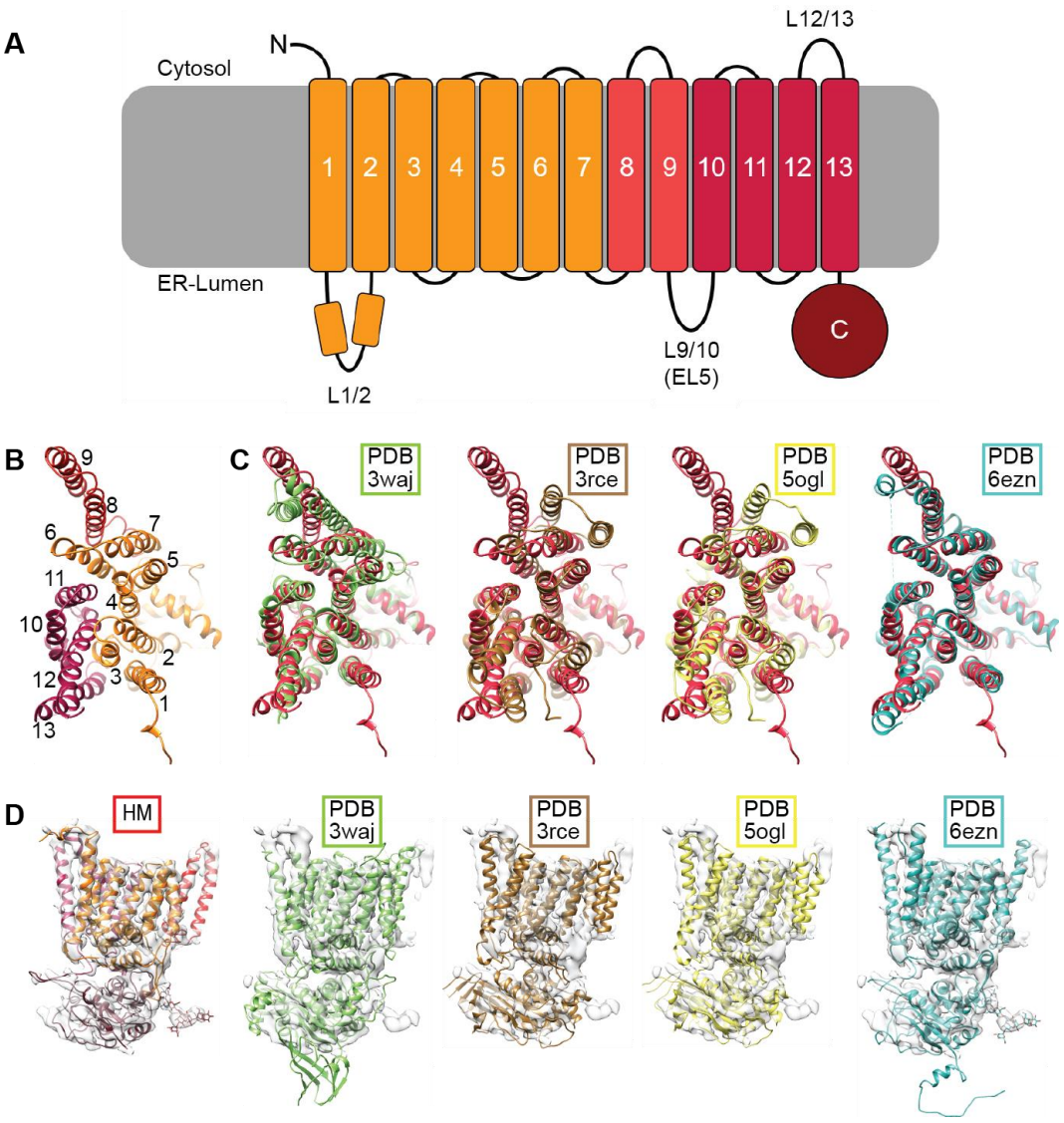

Fig. S6. Homology model of mammalian STT3A. (A) Detailed membrane topology of STT3A. Specific features are indicated. **(B)** Homology model of mammalian STT3A as seen from the cytosol. Order of TM segments is indicated by Arabic numbering (TM1-7 orange, TM8/9 light red, TM10-13 dark red). **(C)** Superposition of the homology model (red) with X-ray structures of archaeal (green, PDB 3waj), bacterial (brown, PDB 3rce; yellow, PDB 5ogl) and yeast (blue, PDB 6ezn) homologs shows a very similar arrangement

of TMs 1-7 and 10-13 and a relocation of TM8-9. **(D)** Fit of the models from **(C)** into the cryo-EM density, low-pass-filtered to 4.0 Å according to local resolution of TM segments.

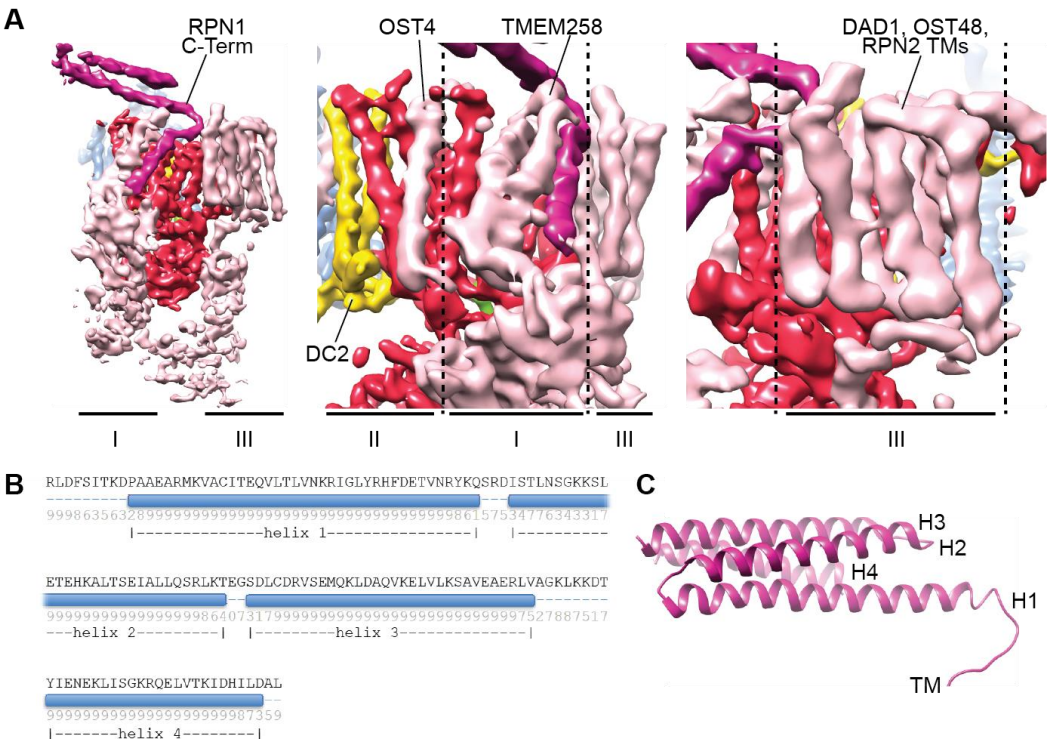

Fig. S7. Identification of known OST subcomplexes. (A) Assignment of biochemically established OST subcomplexes (indicated by Roman numbering). Left: View from the distal side of STT3A (red) reveals bundles of three and seven additional TM-segments, respectively (magenta: RPN1, pale pink: other OST subunits) which display extended luminal portions. Center: The three-TM bundle can be assigned to subcomplex I (RPN1+TMEM258). In addition, the single TM between STT3A TMs 1,3,12 and 13 represents OST4 of subcomplex II (STT3A+DC2+OST4+KCP2). Right: The remaining seven-TM bundle is assigned to subcomplex III (RPN2+DAD1+OST48). **(B)** Secondary structure prediction for the cytosolic RPN1 moiety (residues 458-607, jPred4). The amino acid primary sequence, the secondary structure prediction and prediction confidence are given. **(C)** Backbone model for the cytosolic RPN1 domain based on **(B)** and the density observed in the locally refined P site tRNA containing reconstruction.

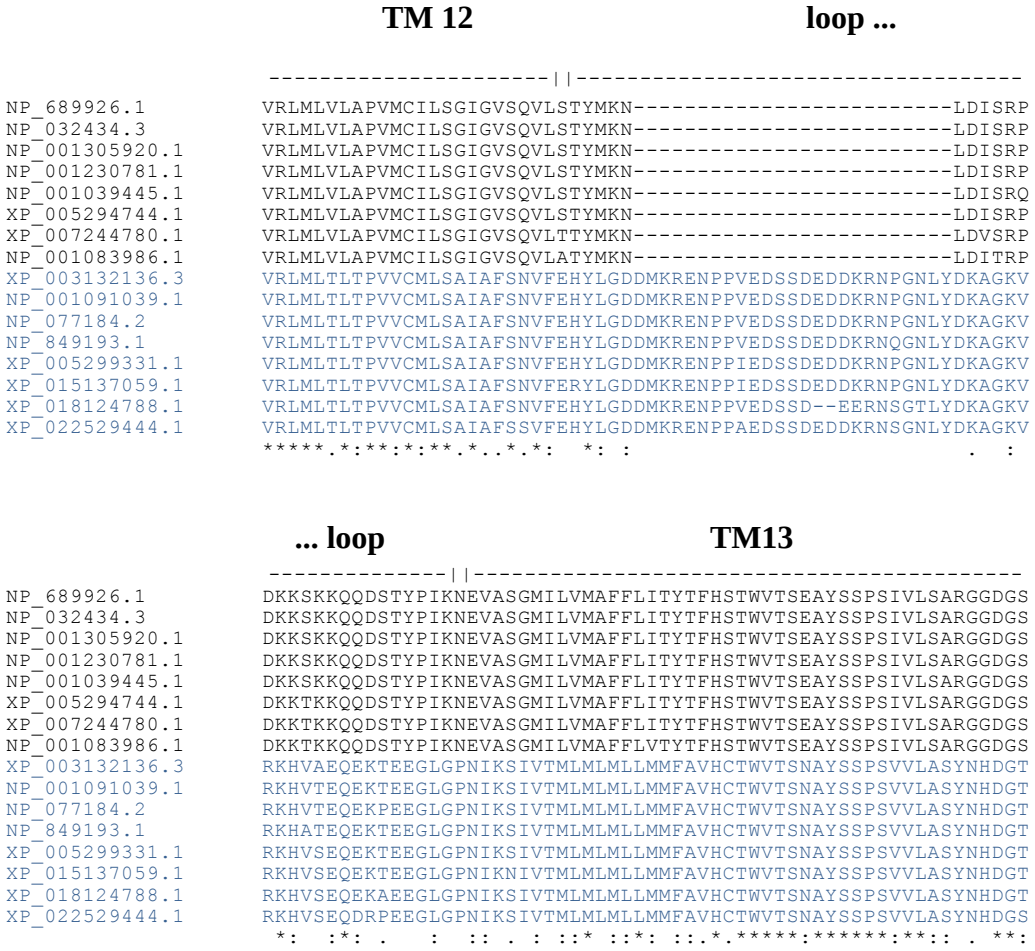

Fig. S8. Diversity of primary sequences for the cytosolic STT3-TM12/13 loop in various metazoan organisms. Residues 404-498 (reference sequence: NP_689926.1) for STT3A and STT3B paralogs are shown in black and blue, respectively. Compared organisms are: Homo sapiens (NP_689926.1, NP_849193.1), Mus musculus (NP_032434.3, NP_077184.2), Bos taurus (NP_001039445.1, NP_001091039.1), Sus scrofa (NP_001230781.1, XP_003132136.3), Gallus gallus (NP_001305920.1, XP_015137059.1), Chrysemys picta (XP_005294744.1, XP_005299331.1), Xenopus laevis (NP_001083986.1, XP_018124788.1), Astyanax mexicanus (XP_007244780.1, XP_022529444.1).

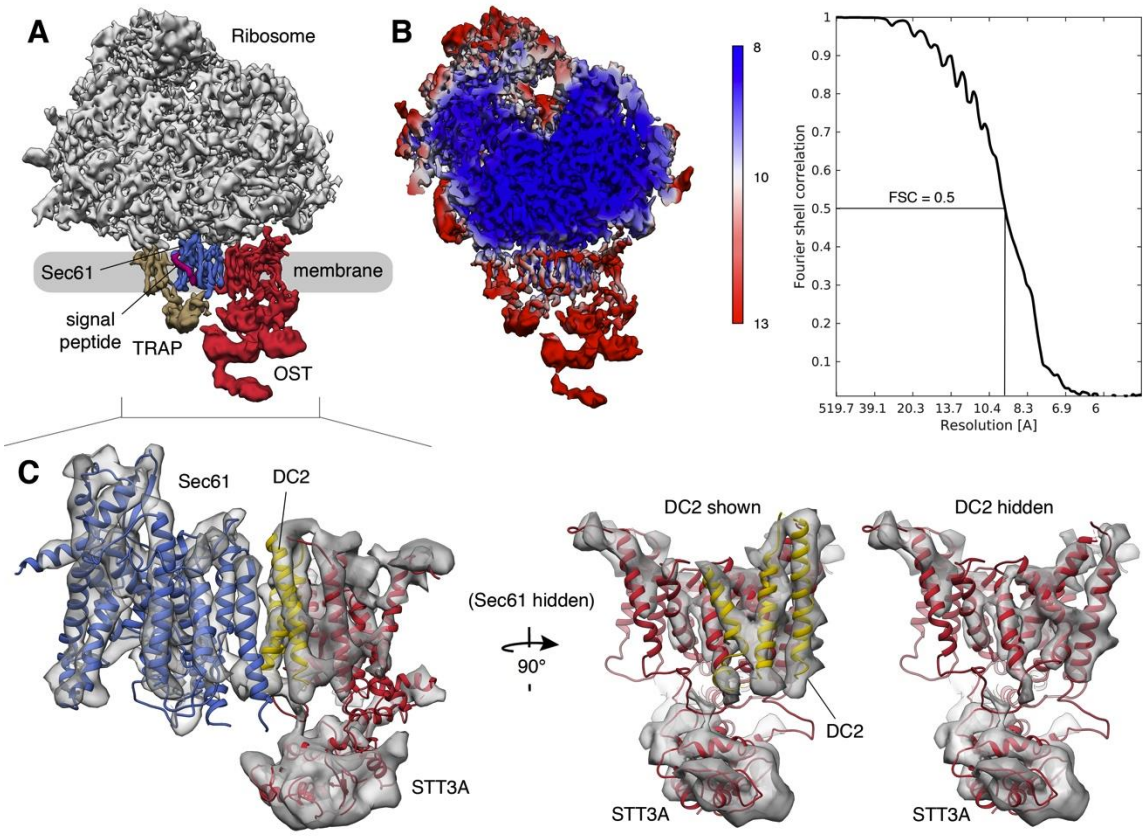

Fig. S9. Improved cryo-ET density of the native ribosome-translocon complex. (A) Overall cryo-ET density of the native ribosome translocon complex. The ribosome (grey) and the translocon constituents Sec61 (blue), TRAP (beige) and OST (red) are shown. Density for a hydrophobic helix intercalated at the lateral gate of Sec61α is depicted in magenta. Density for the ER membrane was omitted for an unobstructed view on translocon constituents. **(B)** Resolution assessment of the cryo-ET density via local resolution estimation (left) and Fourier shell correlation (FSC) of two halves of the data after applying a spherical mask encompassing the ribosomes and membrane-embedded parts of the translocon (right; 9.1 Å at FSC = 0.5). **(C)** Zoom on the isolated Sec61, DC2 and STT3 densities as shown in (A). The atomic models for laterally opened Sec61 (blue), DC2 (yellow) and STT3 (red) are superposed.

Table S1. Primary sequence conservation between STT3A and B paralogs from various metazoan organisms. Sequence identity between STT3A and STT3B paralogs for the sequence ranges covering TMs 10-13 (residues 347-501 of reference sequence NP_689926.1) or TMs 1-9 (residues 7-346 of reference sequence NP_689926.1) are shown. We note that TMs 1-9 are significantly better conserved (~60% identity between paralogs) than the DC2-interacting TMs 10-13 (~39 % identity between paralogs).

Organism		**Sequence IDs (STT3A/B)**	**Identity TMs 10-13 [%]**	**Identity TMs 1-9 [%]**
Mammalia	Homo sapiens	NP_689926.1 NP_849193.1	39.34	60.70
	Mus musculus	NP_032434.3 NP_077184.2	39.34	60.70
	Bos taurus	NP_001039445.1 NP_001091039.1	39.34	60.70
	Sus scrofa	NP_001230781.1 XP_003132136.3	39.34	60.41
Aves	Gallus gallus	NP_001305920.1 XP_015137059.1	38.80	59.82
Reptilia	Chrysemys picta	XP_005294744.1 XP_005299331.1	39.34	59.82
Amphibia	Xenopus laevis	NP_001083986.1 XP_018124788.1	39.34	60.11
Osteichthyes	Astyanax mexicanus	XP_007244780.1 XP_022529444.1	39.89	58.94

Movie S1. Conformational rearrangements of translocon constituents. The movie shows an interpolation from the arrangement of translocon constituents in the "programmed / closed Sec61" state over the "non-programmed / closed Sec61" state to the "non-programmed / laterally open Sec61" state, and back. Models for Sec61 (blue) and OST (DC2: gold, STT3: red, RPN1: violet, additional OST TMs: pink) are shown. During the first cycle, the respective cryo-EM densities are superposed.